Polymer 51 (2010) 5532–5538

Contents lists available at ScienceDirect

Polymer

journal homepage: www.elsevier.com/locate/polymer

# Kinetic study of the II–I phase transition of isotactic polybutene-1

Masanori Maruyama [a], Yusuke Sakamoto [a], Koji Nozaki [a,*], Takashi Yamamoto [a], Hiroshi Kajioka [b], Akihiko Toda [b], Koji Yamada [c]

[a] Department of Physics, Graduate School of Science and Engineering, Yamaguchi University, Yamaguchi 753-8512, Japan
[b] Graduate School of Integrated Arts and Sciences, Hiroshima University, Higashi-Hiroshima 739-8521, Japan
[c] Kawasaki Development Center, SunAllomer Ltd., 3-2, Yako 2-chome, Kawasaki-ku, Kawasaki 210-0863, Japan

ARTICLE INFO

*Article history:*
Received 20 April 2010
Received in revised form
21 September 2010
Accepted 27 September 2010

*Keywords:*
Polybutene-1
Phase transition
Kinetics

ABSTRACT

Kinetics of the solid–solid II–I phase transition of isotactic polybutene-1 was investigated. The fraction $W_I$ of phase I as a function of time $t_{tr}$ during the phase transition was measured by X-ray diffraction at various temperatures $T_{tr}$. The Avrami indices $n$ of the $W_I$–$t_{tr}$ plots are approximately unity for $T_{tr} > 288$ K. A bell-shaped temperature dependence of the transition rate $V$ with the maximum transition rate at 285 K was obtained. The $V$–$T_{tr}$ curve and the Avrami index $n = 1$ suggest that the rate-determining process is primary nucleation. The dependence of $V$ on $T_{tr}$ for $T_{tr} < 283$ K is described by the William–Landel–Ferry (WLF) equation, which shows that the glass transition affects the transition rate. The Avrami index decreases to $n < 1$ for $T_{tr} < 283$ K, indicating a broadened distribution of the transition rate caused by the spatial heterogeneity of the amorphous state at low temperatures near the glass transition. Those evidences at low temperature clearly suggest that the solid–solid phase transition is influenced by the mobility of chain folding, tie chains and cilia in the amorphous between the stacks of lamellar crystals.



## 1. Introduction

Understanding the kinetics of first-order phase transitions such as crystallization, solid–solid phase transitions, etc. is important for materials science and engineering, and this is reflected in many kinetic studies that have been made on first-order phase transitions, and in particular on the topic of crystallization [1–3]. However, with regards to the studies of the kinetics of solid–solid phase transitions, there has been a difficulty of direct observation of transitions, which quite often completes in a short time interval. In recent years, an experimental technique has been developed that makes it possible to investigate the kinetics of first-order solid–solid phase transitions in dielectric materials [4,5], metal alloys [6,7], and other low-molecular-weight materials [8–12]. In long-chain materials and polymers, the solid–solid phase transition is comparatively slow processes, and the kinetics has been studied by time-resolved observation [13–15].

In this article, we present a study of the kinetics of the solid–solid phase transition in a crystal of isotactic polybutene-1 (iPBu-1). The material iPBu-1 is a typical semi-crystalline polyolefin polymer. Because of its good thermal-barrier properties and creep strength, iPBu-1 is widely used as feed-pipe material for hot water pipes. The iPBu-1 crystal exhibits a solid–solid first-order phase transition from phase II to phase I [16,17]; the crystal data of phases I [16,18] and II [19,20] are listed in Table 1.

The II–I phase transition is known to be very slow and needs more than a few days to complete at room temperature. Therefore, partly because of the possible influence on the practical application, the II–I phase transition has been widely investigated [21–29] with the conclusion that it is metastable to the most stable phase transition. Possible free-energy curves of the crystalline phases I and II as well as of the liquid phase (L) are shown in Fig. 1, which also shows the phase-transition behavior. When iPBu-1 is cooled from the liquid state (L) to a temperature below the melting points of phase I ($T_{I-L}$) and phase II ($T_{II-L}$), it first crystallizes into the metastable phase II and subsequently transforms to the most stable phase I. This sequence of phase-transition steps is the result of Ostwald's step rule.

Several experimental studies [24,27] have reported that primary nucleation of phase I in the phase II crystallite is the rate-determining process of the II–I transition. The results of transmission electron microscopy (TEM) [27] studies provide experimental evidence that when one primary nucleus forms in a single phase II crystalline domain, the nucleus quickly grows over the entire single crystalline domain, completing the II–I transition. The temperature dependence of the II–I phase transition rate of iPBu-1 has been measured by means of dilatometry [21,22], and the transition rate as a function of temperature exhibits a bell-shaped curve with

* Corresponding author. Tel.: +81 83 933 5679; fax: +81 83 933 5273.
*E-mail address:* nozaki@yamaguchi-u.ac.jp (K. Nozaki).

0032-3861/$ – see front matter © 2010 Elsevier Ltd. All rights reserved.
doi:10.1016/j.polymer.2010.09.066

**Table 1**
Crystal data for phases I and II of iPBu-1 crystal.

| Phase | Unit cell (space group) | Helix type | *a* (nm) | *c* (nm) | Density (g/cm$^3$) | Melting point (K) |
|---|---|---|---|---|---|---|
| I | Trigonal ($R\bar{3}c$) | 3/1 | 1.77 | 0.65 | 0.95 | 413.0 |
| II | Tetragonal ($P\bar{4}b2$) | 11/3 | 1.46 | 2.12 | 0.91 | 402.4 |

a maximum at room temperature. A similar type of temperature dependence often observed for the polymer crystallization [30], which is limited by the melting point at high temperature and by the glass transition at lower side. For the bell-shaped rate of the II–I phase transition, it is also reasonable that the rate is limited by the II–I transition temperature ($T_{I-II}$) at high-temperature side. On the other hand, at lower temperatures, even for the solid–solid phase transition, it can be possible that the molecular dynamics in the amorphous controls the transition due to the existence of chain foldings, tie chains, and cilia in the amorphous between the stacks of crystalline lamellae. This behavior is considered to be significant at temperatures near the glass-transition temperature, at which the segmental diffusion of the molecules is depressed and the transition is set the lower limit.

In this study, we examine the time evolution of the fraction of a new phase during the solid–solid phase transition at various temperatures $T_{tr}$, and the effect of the glass transition on the transition rate will be discussed. The variation of the phase I fraction $W_I$ with time $t_{tr}$ was measured by using in situ wide angle X-ray diffraction (in situ WAXD). It is known that the II–I phase transition in iPBu-1 homopolymer proceeds at a very slow rate and the transition takes a few days even at room temperature, for which the transition rate is a maximum. In order to examine the transition behavior in a wide temperature range in the time scale accessible for us, we examine the transition of the buten-1-propylene random copolymer (iPBu-1 copolymer), in which the II–I phase transition is accelerated [31].

## 2. Experimental

The iPBu-1 copolymer sample used in this study was provided by SunAllomer Ltd., and contained 5.6 wt% of propylene monomer. The number-average and weight-average molecular weights ($M_n$ and $M_w$, respectively) of the iPBu-1 copolymer sample were $1.22 \times 10^5$ and $5.00 \times 10^5$, respectively. The glass-transition temperature $T_g$ of the sample was about 251 K.

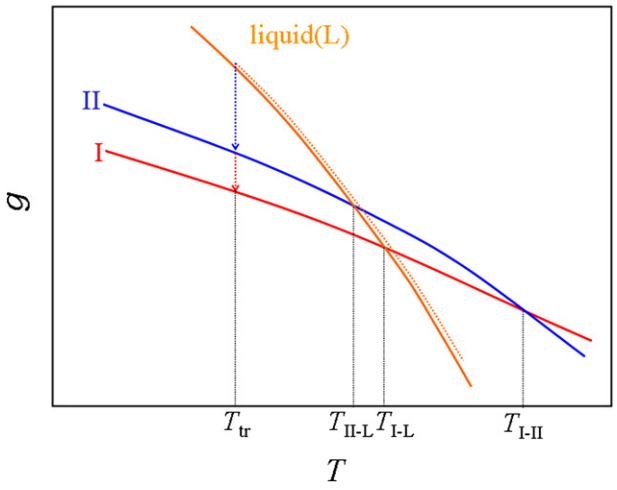


**Fig. 1.** Possible free-energy curves of iPBu-1 and its phase-transition behavior.

The time $t_{tr}$ development of the fraction $W_I$ of phase I during the II–I phase transition was observed via in situ WAXD. About 3 mg of the iPBu-1 copolymer was melted at 433 K for 10 min and was crystallized at 333 K. The II–I phase transition proceeds very slowly at 333 K. After the crystallization process, the sample was rapidly mounted onto the X-ray goniometer. The sample temperature $T_{tr}$ was controlled by flowing temperature-controlled nitrogen gas over the sample by using an Oxford Cryostream Cooler (Oxford Cryosystems), which gives a temperature precision of ±0.5 K. In this way, time-resolved WAXD patterns were collected at each appropriate time period. The X-ray diffraction equipment consisted of a Bruker AXS DIP220 with an image-plate X-ray detector, and monochromatic Cu-Kα radiation was used (40 kV, 250 mA). The exposure time was 5 min for one shot.

## 3. Results and discussion

### 3.1. II–I transition rates and kinetics

Fig. 2 shows X-ray diffraction profiles obtained at $t_{tr} = 0$, 40, 150, 255, and 390 min during the II–I phase transition at 293 K. The 110 Bragg reflection peak of phase I ($110_I$) and the 200 Bragg reflection peak of phase II ($200_{II}$) are observed at $2\theta = 10.1°$ and 12.1°, respectively. The intensity of the 200 Bragg reflection of phase II decreases with time, whereas that of the 110 reflection of phase I increases. Thus, the II–I phase transition is confirmed by WAXD. The fraction $W_I$ of phase I is obtained by the following equation:

$$W_I(t_{tr}) = \frac{I(110_I)}{I(110_I) + \alpha \cdot I(200_{II})}, \quad (1)$$

where $I(110_I)$ and $I(200_{II})$ are the integrated intensities of the $100_I$ and $200_{II}$ reflections, respectively, corrected by the Lorentz-polarization factor. The coefficient $\alpha$ in Eq. (1) is a function of $T_{tr}$ and is given by

$$\alpha(T_{tr}) = \frac{j(110_I) \cdot |F(110_I)|^2 \cdot D(110_I)}{j(200_{II}) \cdot |F(200_{II})|^2 \cdot D(200_{II})}, \quad (2)$$

where $j(110_I)$ and $j(200_{II})$ are the multiplicities of the $110_I$ and $200_{II}$ reflections, $F(110_I)$ and $F(200_{II})$ are the structure factors of the two

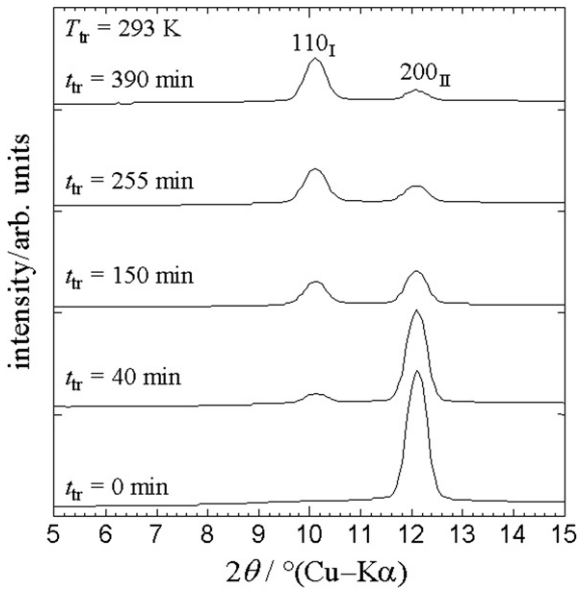


**Fig. 2.** X-ray diffraction profiles at $t_{tr} = 0$, 40, 150, 255, and 390 min during the II–I phase transition at $T_{tr} = 293$ K.

reflections, and $D(110_I)$ and $D(200_{II})$ are the Debye–Waller factors. The multiplicities of the two reflections are $j(110_I) = 6$ and $j(200_{II}) = 4$. Because the crystal-structure detail in phase II has not yet been determined, the structure factor $F(200_{II})$ and the Debye–Waller factor $D(200_{II})$ cannot be calculated. Therefore, under the assumption of the conservation of crystallinity, the value of $\alpha$ at each $T_{tr}$ is estimated from the changes in the integrated intensities of the Bragg reflection peaks with time by using

$$\alpha(T_{tr}) = -[dI(110_I)/dt]/[dI(200_{II})/dt]. \quad (3)$$

Fig. 3 shows time evolution of the fraction $W_I$. The data for $W_I$ vs. $t_{tr}$ in Fig. 3 lie approximately on a curve given by the Avrami equation [32]

$$W_I(t_{tr}) = 1 - \exp\left[-\left(V^* \cdot t_{tr}\right)^n\right], \quad (4)$$

where $V^*$ is a transition rate coefficient and $n$ is an Avrami index. From Eq. (4), we derive

$$\log[-\ln(1 - W_I)] = n \cdot \log V^* + n \cdot \log t_{tr}. \quad (5)$$

Fig. 4 shows Avrami plots of $W_I$ shown in Fig. 3. All data sets for $T_{tr}$ lie on individual lines. Thus, the II–I phase transition of iPBu-1 copolymer can be discussed on the basis of Avrami's theory [32].

Fig. 5 shows the dependence on $T_{tr}$ of the Avrami index $n$ obtained from the plots, such as shown in Fig. 3, by Eq. (4). According to Avrami's theory, the index $n$ exhibits the geometric growth mode of a new phase (phase I) from a matrix phase (phase II) during a phase transition. The values of $n$ at temperatures above 288 K are about unity, as has been reported for homopolymer [26]. For $n = 1$, a possible characteristic process of the II–I phase transition is one-dimensional growth from multiple primary nuclei (heterogeneous nucleation) or homogeneous primary nucleation and "zero-dimensional growth". In the previous study by Kopp et al. [27], the formation of a single primary nucleus of phase I and its rapid three-dimensional growth in a single crystalline domain of phase II were confirmed, as mentioned in the Introduction. Thus, it is concluded that the geometric image of the II–I phase transition of iPBu-1 copolymer is homogeneous nucleation and "zero-dimensional growth". Generally, the iPBu-1 copolymer consists of a great number of small crystalline lamellar domains. When a single primary nucleus forms in a crystalline domain, the nucleus rapidly grows over the domain. Then, the fraction of the remaining phase II domains decreases sporadically with the primary nucleation in the domains. In other words, the rate-determining process of the II–I phase transition of the iPBu-1 copolymer at temperatures above 288 K is primary nucleation. For temperatures below 288 K, on the other hand, the Avrami index $n$ becomes lower than one with decreasing temperature. The Avrami model of the homogeneous nucleation fails to explain the index $n < 1$, the physical meaning of which will be discussed in a subsequent section in detail.

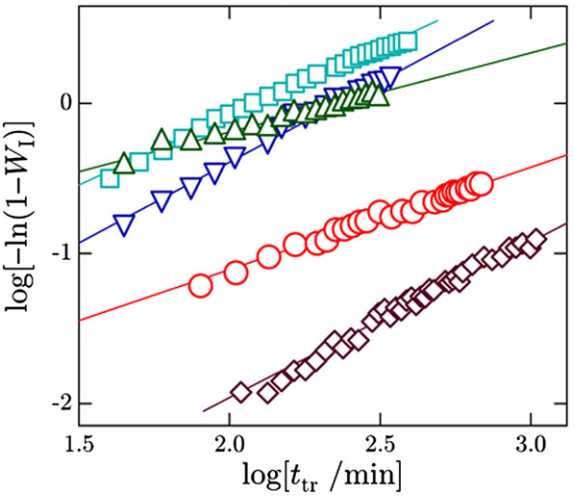


**Fig. 4.** Avrami plots of $W_I$ shown in Fig. 3: $T_{tr} = 258$ (○), 268 (△), 293 (□) 308 (▽), and 313 K (◇) with the slopes of the fitting lines 0.68, 0.59, 0.92, 1.08, and 1.04, respectively.

Fig. 6 shows the temperature dependence of the II–I transition rate of the iPBu-1 copolymer. The transition rate exhibits a bell-shaped temperature dependence with a maximum near 285 K, similar to what is found for the iPBu-1 homopolymer [21,22]. Assuming that primary nucleation controls the II–I transition rate, then the II–I transition rate must be proportional to the primary nucleation rate.

In this case, the temperature dependence of the transition rate is described by the following theoretical equation:

$$V(T_{tr}) = V_0' \cdot \beta(T_{tr}) \cdot \exp\left(-\frac{\Delta G^*}{k_B \cdot T_{tr}}\right), \quad (6)$$

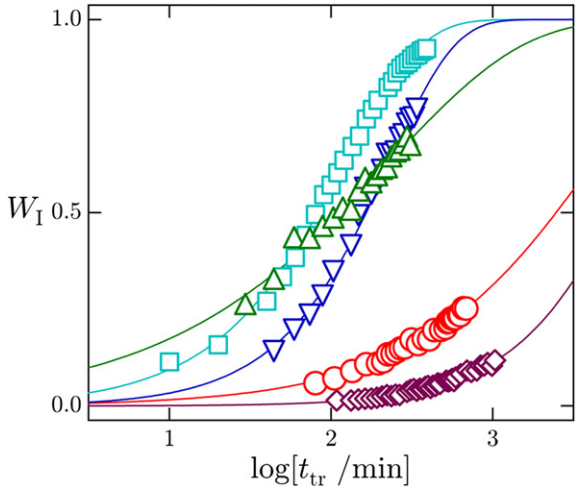


**Fig. 3.** Time evolution of the fraction of phase I ($W_I$) at $T_{tr} = 258$ (○), 268 (△), 293 (□) 308 (▽), and 313 K (◇). The curved lines represent the fitting by Eq. (4).

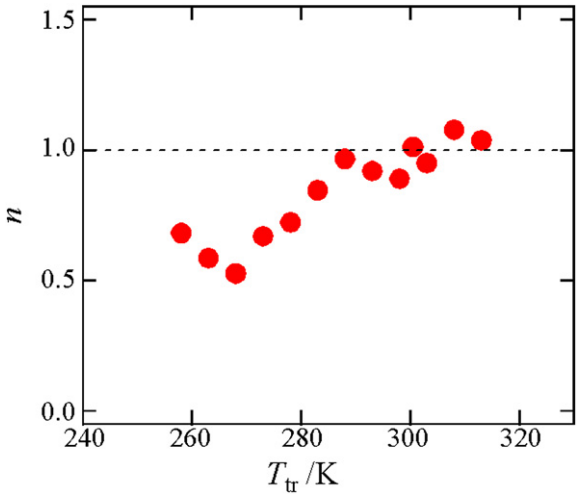


**Fig. 5.** Dependence of Avrami index $n$ on $T_{tr}$, obtained by fitting of the plots, such as shown in Fig. 3 by Eq. (4).

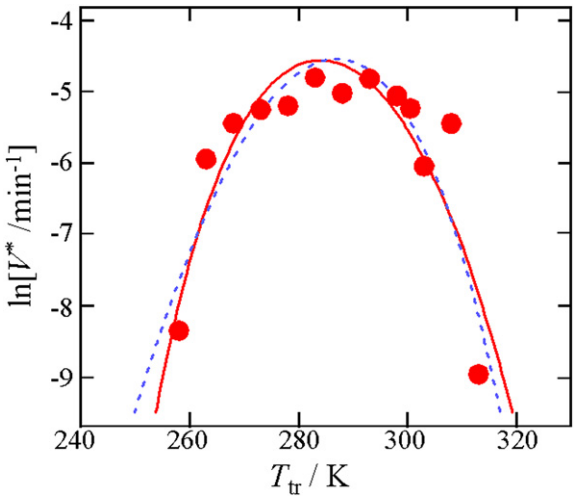


**Fig. 6.** $T_{tr}$ dependence of the transition rate $V^*$ obtained by fitting of the plots, such as shown in Fig. 3 by Eq. (4). The broken and solid curves represent the results of fitting by Eqs. (16) and (17) for $T_{I-II} = 420$ K, respectively.

where $V_0'$ is a constant, $\beta(T_{tr})$ is a molecular diffusion factor, $\Delta G^*$ is the free energy for formation of a critical nucleus, and $k_B$ is the Boltzmann constant. The exponential factor of the critical nucleus in Eq. (6) mainly determines the behavior of $V$ on the high-temperature side of the maximum in Fig. 6. According to the general nucleation theory, $\Delta G^*$ for three-dimensional primary nucleation is in the following form:

$$\Delta G^* \equiv \frac{B}{f\left(\Delta T^2\right)}, \tag{7}$$

where $B$ is a constant, $\Delta T \equiv T_{I-II} - T_{tr}$ is the degree of supercooling from the transition temperature $T_{I-II}$, and $f(\Delta T^2)$ is a function of $\Delta T$. At low supercooling, $f(\Delta T^2)$ can be regarded just as $\Delta T^2$. But for higher supercooling as in the present case of $\Delta T > 100$ K, due to the temperature dependences of the heat and entropy of transition, we need to consider additional terms. Under the assumption of constant heat capacity difference between phase II and I, $f(\Delta T^2)$ is approximately expressed as

$$f\left(\Delta T^2\right) \cong \Delta T^2 - 2A_0\Delta T^3 + A_0^2\Delta T^4, \tag{8}$$

where $A_0$ is given by the difference in the heat capacities [33] of phase II ($c_{II,p}$) and of phase I ($c_{I,p}$) and by the heat of transition ($\Delta h_{I-II}$), as follows:

$$A_0 \equiv \frac{\Delta c_{I-II,p}}{2\Delta h_{I-II}}, \tag{9}$$

$$\Delta c_{I-II,p} \equiv c_{II,p}(T_{I-II}) - c_{I,p}(T_{I-II}) = 0.310 \text{ J/g K}, \tag{10}$$

$$\Delta h_{I-II}(T_{I-II}) \cong \Delta h_{I-L}(T_{I-L}) - \Delta h_{II-L}(T_{II-L}) = 118 \text{ J/g}, \tag{11}$$

where the heat of fusion of the respective phases at the transition temperature $T_{I-II}$ is approximated by the value at the respective melting points, $\Delta h_{I-L}(T_{I-L})$ and $\Delta h_{II-L}(T_{II-L})$, which were obtained by differential scanning calorimetry. It is noted that approximately form of $f(\Delta T^2)$ in Eq. (8) gives us the very close value to that obtained with the following well-known correction factor proposed by Hoffman [34] for polymer crystallization,

$$f_{Hoff}\left(\Delta T^2\right) \cong \left(\frac{2T_{tr}}{T_{I-II} + T_{tr}}\Delta T\right)^2. \tag{12}$$

Assuming that the primary nucleus of phase I is a hexagonal prism, where the side surfaces are the (100) and its five equivalent planes and (001) plane is the basal plane, the constant $B$ in Eq. (7) is given by

$$B = \frac{16\sqrt{3}\sigma_s^2 \cdot \sigma_e T_{I-II}^2}{\Delta h_{I-II}^2}, \tag{13}$$

where $\sigma_s$ is the surface free energy of the {100} interface between phases I and II, and $\sigma_e$ is the surface free energy of the {001} interface.

With regard to the molecular diffusion factor $\beta(T_{tr})$ in Eq. (6), since the transformation proceeds in the solid phase, the applicability of the following Arrhenius-type temperature dependence should be examined first,

$$\beta(T_{tr}) \propto \exp\left(-\frac{E}{RT_{tr}}\right), \tag{14}$$

where $E$ is activation energy for molecular diffusion and $R$ is the gas constant. In the present case, however, the observed temperature dependence of $V$ is not explained well by Eq. (14) as shown below. Therefore, we apply the William–Landel–Ferry (WLF) type [35–38] as the temperature dependence for $\beta(T_{tr})$,

$$\beta(T_{tr}) \propto \exp\left[-\frac{U^*}{R(T_{tr} - T_V)}\right], \tag{15}$$

where $U^*$ is the effective activation energy for chain diffusion and $T_V$ is the Vogel temperature, which is experimentally given as $T_V \approx T_g - 51$ K for the viscosity and molecular mobility in the liquid state. The WLF factor introduces the effect on chain diffusion of the glass transition of polymer molecules and appears to explain the temperature dependence of the growth rate of polymer crystals [39]. By using Eqs. (7) and (14) or (15), Eq. (6) becomes

$$V(T_{tr}) = V_0 \exp\left(-\frac{E}{RT_{tr}}\right)\exp\left[-\frac{B}{k_B T_{tr} f(\Delta T^2)}\right], \tag{16}$$

$$V(T_{tr}) = V_0 \exp\left(-\frac{U^*}{R(T_{tr} - T_V)}\right)\exp\left[-\frac{B}{k_B T_{tr} f(\Delta T^2)}\right], \tag{17}$$

for the mobility factors of Arrhenius and WLF type, respectively, where $V_0$ is a constant.

The observed temperature dependence of the II–I transition rate $V^*$ was fitted by Eqs. (16) and (17). The optimizing parameters are $V_0$, $E$, $B$, and $T_{I-II}$ for the Arrhenius type and $V_0$, $U^*$, $T_V$, $B$, and $T_{I-II}$ for the WLF type, respectively. Among them, the transition temperature ($T_{I-II}$) should be higher than the melting point of phase I ($T_{I-L}$), as shown in schematic diagram of Fig. 1. We have fixed $T_{I-II}$ in the range of 410–460 K and examined the optimization of the fitting with other parameters. The result of the fitting for $T_{I-II} = 420$ K is shown in Figs. 6 and 7. The fitting was satisfactory for the examined range of $T_{I-II}$ and the parameters obtained for the WLF type are shown in Fig. 8. This result indicates that the rate-determining process of the II–I transition is primary nucleation, and is consistent with the result of the Avrami analysis of time evolution.

Assuming that $\sigma_e = \sigma_s$ and by using c.a. $B/k_B = 6.7 \times 10^7$ K$^3$ optimized for $T_{I-II} = 420$ K in Fig. 8, the surface free energies

$$\sigma_e = \sigma_s = 1.3 \times 10^{-2} \text{ J/m}^2 \tag{18}$$

are obtained. According to the kinetic study on the crystallization of iPBu-1 by Yamashita et al. [20], the surface free energy of the end interface between phase I and the amorphous phase is

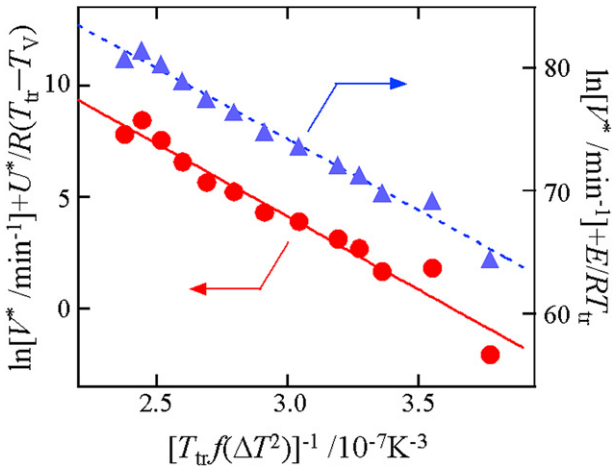


**Fig. 7.** Plots of $\ln V^* + U^*/R(T_{tr} - T_V)$ and $\ln V^* + E/RT_{tr}$ vs. $[T_{tr}f(\Delta T^2)]^{-1}$. The broken and solid lines represent the result of fitting by Eqs. (16) and (17) for $T_{I-II} = 420$ K, respectively.

$\sigma_{e,I-L} = 5.4 \times 10^{-2}$ J/m$^2$, and that between phase II and the amorphous phase is $\sigma_{e,II-L} = 5.7 \times 10^{-2}$ J/m$^2$. Compared with those values by Yamashita et al. [20], the $\sigma_e$ and $\sigma_s$ values determined in this work are in the same order. In the present case, the surface free energies $\sigma_e$ and $\sigma_s$ correspond to the crystal–crystal (I–II) interface. On the other hand, $\sigma_{e,I-L}$ and $\sigma_{e,II-L}$ are the surface free energies between the crystalline and liquid phases. Therefore, it is easy to understand that $\sigma_e$ and $\sigma_s$ are smaller than $\sigma_{e,I-L}$ and $\sigma_{e,II-L}$. Thus, we consider the surface free energies obtained in this work to be reasonable values.

### 3.2. Effect of molecular diffusion on the II–I transition rate

In Figs. 6 and 7, the results of the fitting by Eq. (16) of the Arrhenius type are shown as well as fitting by Eq. (17) of the WLF type. Although the fitting is satisfactory also for the Arrhenius type, there is a serious problem in the prefactor $V_0$. As seen in Fig. 7, $V_0$ of Arrhenius type becomes unacceptably high; e.g. for $T_{I-II} = 420$ K, $V_0 > 10^{47}$ min$^{-1}$ which is higher than the attempt frequency $k_B T_{tr}/h \sim 6 \times 10^{12}$ Hz by more than $10^{30}$, where $h$ is a Planck's constant.

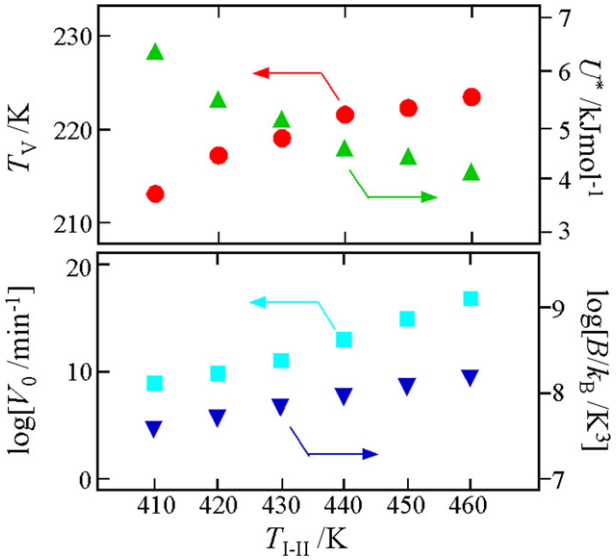


**Fig. 8.** Kinetic parameters, $T_V$ (●), $U^*$ (▲), $V_0$ (■), and $B/k_B$ (▼), obtained by fitting of the plots such as shown in Fig. 6 by Eq. (17) for the respective $T_{I-II}$.

The factor will also include large number of nucleation sites, but for the primary nucleation in the crystal domains of submicron size, the factor of $10^{30}$ will be unacceptable. For this reason, the mobility factor represented by the Arrhenius type has been dismissed. On the other hand, as shown in Fig. 8, $V_0$ of the WLF type will be within the acceptable range not far from $k_B T_{tr}/h$.

It is well know that the WLF equation (Eq. (15)) is based on self-diffusion in a polymer liquid [35–38] and the segmental motion of molecules in the amorphous phase. Furthermore, the effect of the glass transition of polymer molecules on chain diffusion is taken into account by the WLF formula. The phase transition seems to freeze at the Vogel temperature. Thus, this result indicates that the II–I transition rate is affected by the glass transition of the molecules.

For viscosity measurements, the effective activation energy of chain diffusion, $U^* \sim 17$ kJ/mol, and the Vogel temperature, $T_V \approx T_g - 51$ K, are usually used as "universal" constants [36]. The obtained values of c.a. $U^* = 5.5$ kJ/mol and $T_V = 217 \approx T_g - 34$ K (with $T_g = 251$ K) for $T_{I-II} = 420$ K in this work seem to be out of the rage for the viscosity. For polymer crystallization, however, $U^* \sim 6.3$ kJ/mol and $T_V \approx T_g - 30$ K are often used as optimized set parameters [34]. If anything, $U^* = 5.5$ kJ/mol and $T_V = 217$ K in this case are comparable to the latter values reported for polymer crystallization.

The glass transition is generally peculiar to amorphous molecules. Although the II–I phase transition is a solid-to-solid phase transition that occurs in the crystalline region, the transition process needs the diffusion of chain segments in the amorphous region by following reason. The crystalline polymer material has a stacked lamellar structure that alternates between the crystalline lamella and the amorphous lamella. Some molecules, such as "cilia" and "tie" molecules, pass through both the crystalline and amorphous phases alike, and molecular rearrangement in the crystalline lamella must accompany the molecular motion in the amorphous region. If the mobility of chain segments in the amorphous region decreases with decreasing temperature because of the glass transition, the movement of chain segments in the crystalline region may be regulated, too. The existence of rigid amorphous fraction at the interface of the crystal and amorphous phases may also contribute the regulation [40,41].

Another scenario may be proposed to explain the effect of the glass transition on the transition rate at low temperature. Phase II is typical CONDIS crystal [42,43], in which the molecular packing is loose and the molecules diffuse by hopping between different conformational states. In such an environment, the phenomenon of freezing the molecular motion is similar to the glass transition and is expected to appear. The glass-transition-like behavior may lower the phase-transition rate. Further investigations are required to substantiate this speculation.

### 3.3. Effect of glass transition on the II–I transition rate

The present study makes it clear that the Avrami index becomes lower than unity with decreasing temperature. In studies on the glass transition, it is often confirmed that relaxation processes, such as dielectric relaxation, mechanical relaxation, etc., in supercooled liquids at temperatures near the glass-transition temperature can be described by a stretched-exponential form of the relaxation function $\varphi(t)$:

$$\varphi(t) = \exp\left[-\left(\frac{t}{\tau}\right)^{\gamma}\right], \tag{19}$$

where $\gamma$ is an index ($0 < \gamma < 1$), and $\tau$ is a characteristic relaxation time [38,44,45]. The stretched-exponential behavior of the

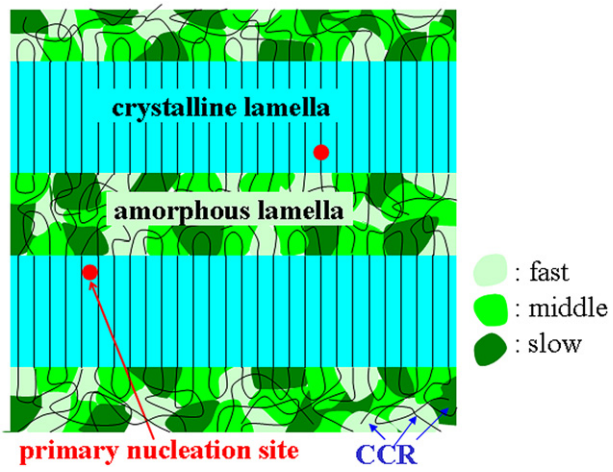


**Fig. 9.** Cooperatively rearranging regions (CRRs) in the amorphous lamella.

relaxation is explained by the spatial heterogeneity of the velocity of molecular segmental motion; i.e. the more broadened relaxation-time distribution corresponds to the smaller index, $\gamma < 1$ [46]. For the transition rate $V$, the index $n < 1$ in Eq. (4) can also be interpreted as stretched-exponential behavior; in this case the behavior arises from the broadened distribution of the transition rate $V$.

Generally, in many types of supercooled polymer liquids, spatial heterogeneity is observed at temperatures near the glass-transition temperature, which may be explained by the concept of cooperatively rearranging regions (CRRs) [46,47], as shown in Fig. 9.

According to this concept, the entire amorphous region is divided into many CRRs that include several chain segments moving cooperatively; the velocity in one CRR is different from that in another CRR. In this way, the spatial heterogeneity appears in the amorphous region. The present results indicate that the II–I transition rate in one crystalline lamella is controlled by the changing velocity of the surrounding amorphous molecules around the primary nucleation site at low temperatures near the glass-transition temperature. Therefore, we suggest that the broadened distribution of $V$ is caused by the spatial heterogeneity of the amorphous region.

The sample used in this work was the bulk one. The II–I phase transition of iPBu-1 is a phenomenon which occurs in the crystalline region. Therefore, the transition can be observed for a single crystal sample as well as for a bulk sample [27,48]. However, there is a possibility that the II–I phase-transition rate for a perfect single crystal may be different from that for a bulk sample. As mentioned above, the experimental results for the bulk sample evidently show that the solid–solid phase transition in the crystal seems to be influenced by the glass transition in the surrounding amorphous molecules. Since it is impossible to apply the same method used in this work to the measurement of the transition rate for a single crystal sample, the direct comparison between the II–I transition rates in a bulk system and a single crystal here. Even though an isolated single lamellar crystal is used, the amorphous-like chain segments, which are for example the chain foldings, the cilia molecules, are considered to remain at the end surface of it. Therefore, it is considered to be difficult to measure the transition rate for a pure bare single crystal. One interesting experimental result of the II–I transition rates of single lamellar crystals was shown by Lü and Yang [49]. According to them, the II–I phase-transition time of iPBu-1 seems to be generally prolonged from 9 days for carbon-uncoated single lamellar crystal samples to 120 days for carbon-coated samples. The former is same order as our data for a bulk sample. They also concluded that this phenomenon is attributed to a surface fixing effect of evaporated carbon. The confinement of the mobility of the local amorphous-like chain segment at the crystal surface seems to retard the phase transition. This concept is considered to be very similar to our conclusion.

## 4. Conclusion

We have presented a study of the kinetics of the II–I phase transition of iPBu-1 crystals, in which we measured the dependence of the transition period $t_{tr}$ on the fraction $W_I$ of phase I crystal. For the II–I phase transition of iPBu-1 at high temperatures, we find through an Avrami analysis of $W_I(t_{tr})$ that the Avrami indices $n \sim 1$. This indicates that the rate-determining process of the II–I phase transition of iPBu-1 is primary nucleation. The transition rate $V$ at various temperatures $T_{tr}$ was estimated from the time evolution of $W_I(t_{tr})$. The dependence on $T_{tr}$ of $V$ gives a bell-shaped curve with a maximum at 285 K. This result is thoroughly explained by the combination of the nucleation theory and the WLF equation.

From the $V$–$T_{tr}$ behavior at temperatures above the $V(T_{tr})$ maximum, we reconfirm that the rate-determining process of the transition is primary nucleation. However, the $V$–$T_{tr}$ behavior in the low-temperature region below the maximum is well described by the WLF equation, which predicts the freeze of the phase transition at the Vogel temperature $T_V$. This suggests that the II–I phase transition in the low-temperature region is affected by the glass transition. At low temperatures, the time evolution is expressed by a stretched-exponential function, indicating a broadened distribution of the transition rate. This result indicates that the II–I transition rate at a low temperature is affected by the spatial heterogeneity of the molecular motion, which is peculiar to the glass transition.

## Acknowledgements

This work was partially supported by KAKENHI (Grant-in-Aid for Scientific Research) on the Priority Area “Soft Matter Physics” from the Ministry of Education, Culture, Sports, Science and Technology of Japan.

## References

[1] Turnbull D, Cormia RL. J Chem Phys 1961;40:820–31.
[2] Cormia RL, Price FP, Turnbull D. J Chem Phys 1962;37:1333–9.
[3] Koutsky JA, Walton AG, Baer E. J Appl Phys 1967;38:1832–9.
[4] Yamada Y. Ferroelectrics 1981;35:51–6.
[5] Komori S, Hayase S, Terauchi H. J Phys Condens Matter 1989;1:3789–800.
[6] Noda Y, Nishihara S, Yamada Y. J Phys Soc Jpn 1984;53:4241–9.
[7] Shannon Jr RF, Nagler SE, Harkless CR, Nicklow RM. Phys Rev B 1992;46:40–54.
[8] Hamaya N, Yamada Y, Axe JD, Belanger DP, Shapiro SM. Phys Rev B 1986;33:7770–6.
[9] Axe JD, Yamada Y. Phys Rev B 1986;34:1599–606.
[10] Iwasaki H, Matsuo Y, Ohshima K, Hashimoto S. J Appl Cryst 1990;23:509–14.
[11] Tadakuma M, Tajima K, Masada G. J Phys Soc Jpn 1995;64:2074–80.
[12] Kakeshita T, Kuroiwa K, Shimizu K, Ikeda T, Yamaguchi A, Date M. Mater Trans JIM 1993;34:423–8.
[13] Nozaki K, Hikosaka M. Jpn J Appl Phys 1998;37:3450–6.
[14] Nozaki K, Hikosaka M. J Mater Sci 2000;35:1239–52.
[15] Nozaki K, Munekane M, Hikosaka M, Yamamoto T. Jpn J Appl Phys 2001;40:6918–26.
[16] Natta G, Corradini P. Nuovo Cimento Suppl 1960;15:40–51.
[17] Natta G, Corradini P, Bassi IW. Nuovo Cimento Suppl 1969;15:52–67.
[18] Yamashita M, Hoshino A, Kato M. J Polym Sci B 2006;44:684–97.
[19] Tashiro K, Miyashita T, Chatani Y, Tadokoro H. Polymer Preprints Jpn 1998;47(14):3869–70.
[20] Yamashita M, Miyaji H, Izumi K, Hoshino A. Poly J 2004;36:226–37.
[21] Boor Jr J, Mitchell C. J Polym Sci A 1963;1:59–84.
[22] Danusso F, Gianotti G. Makromol Chem 1965;88:149–58.
[23] Oda T, Maeda M, Hibi T, Watanabe S. Kobunshi Ronbunshu 1974;31(3):129–34.
[24] Gohil RM, Miles MJ, Petermann J. J Macromol Sci Phys B 1982;21(2):189–201.
[25] Fujiwara Y. Polym Bull 1985;13:253–8.

[26] Chau KW, Yang YC, Geil PH. J Mater Sci 1986;21:3002–14.
[27] Kopp S, Wittmann JC, Lotz B. J Mater Sci 1994;29:6159–66.
[28] Holland VF, Miller RL. J Appl Phys 1964;35:3241–8.
[29] Lorenzo MLD, Righetti MC, Wunderlich B. Macromolecules 2009;42(23): 9312–20.
[30] Laurtzen Jr JI, Hoffman JD. J Res Nat Bur Std A Phys Chem 1960;64A:73–102.
[31] Turner Jones A. Polymer 1966;7:23–59.
[32] Avrami M. J Chem Phys 1940;8:212–24.
[33] Winski H, Grewer T. J Polym Sci C 1964;6:33–41.
[34] Hoffman JD, Davis GT, Lauritzen Jr JI. In: Hannay NB, editor. Treatise on solid state chemistry, vol. 3. New York: Plenum Press; 1979. p. 497–614 [chapter 7].
[35] Vogel H. Phys Z 1921;22:645–6.
[36] Fulcher GS. J Am Ceram Soc 1925;8:339–55.
[37] Williams ML, Landel RF, Ferry JD. J Am Chem Soc 1955;77:3701–7.
[38] Debenedetti PG, Stillinger FH. Nature 2001;410:259–67.
[39] Clark EJ, Hoffman JD. Macromolecules 1984;17:878–85.
[40] Menczel J, Wunderlich B. J Polym Sci Polym Lett 1981;19:261–4.
[41] Suzuki H, Grebowicz J, Wunderlich B. Br Polym J 1985;17:1–3.
[42] Wunderlich B, Grebowicz J. Adv Polym Sci 1984;60/61:1–59.
[43] Miyoshi T, Hayashi S, Imashiro F, Kaito A. Macromolecules 2002;35(15): 6060–3.
[44] Kohlrausch R. Ann Phys Chem (Leipzig) 1974;91:179–214.
[45] Williams G, Watts DC. Trans Faraday Soc 1970;66:80–5.
[46] Kanaya T, Kaji K. Adv Polym Sci 2001;154:88–141.
[47] Adam G, Gibbs JH. J Chem Phys 1965;43(1):139–46.
[48] Tosaka M, Kamijo T, Tsuji M, Kojiya S, Ogawa T, Isoda S, Kobayasi T. Macromolecules 2000;33:9666–72.
[49] Lü K, Yang D. Polym Bull 2007;58:731–6.